Reconstruction and Web Distribution of Measurable Arterial Models

A. Giachetti, M. Tuveri, M. D. and G. Zanetti

CRS4 - VI Strada Ovest, Z.I. Macchiareddu, Uta(CA), Italy
e-mail giach@crs4.it

Abstract

In this paper a novel framework for the segmentation, 3D reconstruction and web distribution of vessel structures specifically tailored to the assessment of Abdominal Aortic Aneurysms for endovascular surgery planning is presented. Deformable models are used for segmentation, while VRML97 and ECMA scripting are used to obtain models that are not only viewable from any VRML97 enabled browser, but that also allow users to perform, directly from standard web browsers, guided measurements of geometrical parameters, relevant to surgical planning.

Introduction

In the near future a large amount of medical data will be transmitted across Internet for remote diagnosis, electronic patient records retrieval, home care, etc.. Images, annotations and texts can be easily transmitted with standard protocols and can be viewed by medical doctors everywhere by using common web browsers. Many examples of web based telemedicine have been proposed and presented in conference papers [Piqueras and Carreño, 1998, Laxminarayan, 2000, Brelstaff et al., 2000]. On the other hand, there are few examples in literature relative to the distribution via Web of 3D

models of organs, and they are not usually tailored to real clinical needs or diagnostic purposes. Typically these models are used only for qualitative study or to implement simple surgical simulators, e.g. [John et al., 1999], albeit current technology limitations force a strong simplification of the procedures being simulated. There are, however, simple applications where current 3D reconstruction and Web technologies can be harnessed to provide a clinically useful tool. One of these applications is the measurement of all the geometric parameters necessary for the planning of endovascular repair of abdominal aortic aneurysms. Endovascular repair is a modern technique, minimally invasive, in which a graft or stent is placed within the abdominal blood vessel through a small incision made in the groin. The stent-graft relines the blood vessel and relieves the pressure of the aneurysm. This technique [Parodi et al., 1991] requires a precise knowledge of distances, dimensions, radii and angles of the vessel region to be treated, and the traditional method of using 2D projections to perform these measurements can lead to large errors [Baskin et al., 1996]. Three dimensional models of vessels can provide surgeons with better quantitative estimates, that can be used, e.g., to measure position and size of aneurysms, to locate stenoses and plaques, and, once it is decided that surgery is necessary, to choose the most appropriate endovascular prostheses and to plan a surgical intervention.

If we consider the fact that, even if minimally invasive, these surgical procedures cause the death of about 1% of the patients and that prostheses are costly objects, we can understand that the development of systems enabling surgeons to quantitatively analyze 3D models of the region to be treated can be very useful, especially if these systems do not require the surgical unit to acquire dedicated hardware and software and – even more important – specialized personnel.

In this paper we describe a new system for the 3D reconstruction and distribution on the net of models for vessels structures. The system is specifically designed to support guided measurements of parameters of medical interest. Once fully validated, the

technology described here could be used by specialized service centers to provide, in a cost-effective way, surgical support through 3D based measurements. Commercial tools for surgical planning or 3D analysis have been developed and are currently tested or used [Vital Images, Voxar], research on segmentation and data fusion and comparing have been proposed, see, for example [Gering et al., 2001] using XML based technology to encode data. All these systems, however, assume the installation of a specialized workstation at the radiological site and assign to the radiologist the use of, often complex, software tools to perform segmentation, volume rendering and measurements. This, as pointed out in [Sato et al., 1997], requires the presence of well-informed personnel at each site, something that can be economically feasible only at the largest radiological sites.

The system described in this paper assumes a completely different work organization, that delegates to specialized centers all the technical work related to segmentation and geometry reconstruction, and lets the local surgeon concentrate on surgical planning using 3D patient specific models securely delivered via the net. This approach removes the need for personnel specifically trained for image processing at the location were the images are acquired, as well as the need for expensive additional modules to be installed on the imaging modalities. Moreover, it provides a natural support for remote consulting. Fig. 1 shows the expected service model: the diagnostic center can send DICOM3 datasets through the net to the elaboration center, and after a few hours, the surgeons can browse, using their standard PC, the resulting VRML97 model and perform guided measurements. Differently from other similar services currently available [Medical Media System, 2000], this new system is based on open standards, does not require specialized software on the client side and it is specifically designed to operate within Internet, allowing the use of encryption, reducing costs and having a good integration with other information system, like electronic patient records. In this paper we describe the surgical application chosen, customization of different segmentation techniques realized for the specific task, a compar-

ison of segmentation techniques, the techniques used to build of the on line measurement support and the first validation results. The paper is structured as follows: Section 1 introduces the problem of Abdominal Aortic Aneurysm measurement, Section 2 presents the segmentation procedure developed to build the vessel models. Section 3 describes the generation of VRML97 model supporting remote measurement useful for surgical planning and prosthesis selection. Section 4 shows the results of experiments aimed to compare and validate the segmentation techniques.

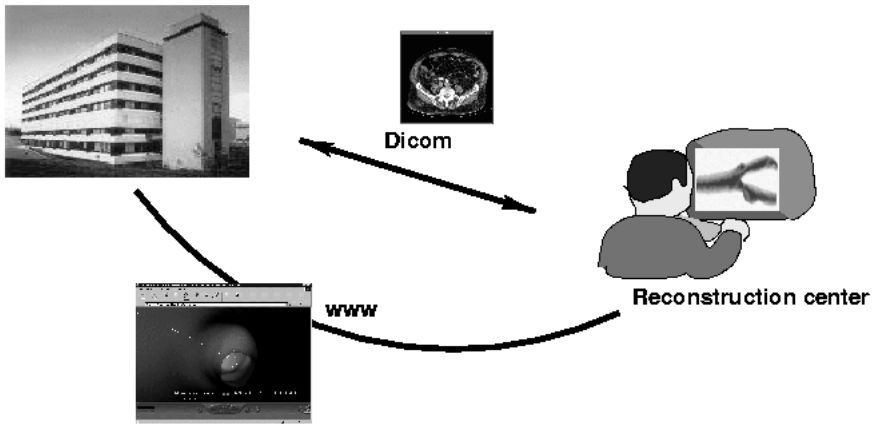

Figure 1: The VRML97 measurable model service: a diagnostic center can send images to the reconstruction center, and a few hours after, a 3D model with guided measurement support is available on the net.

1 Aortic aneurysms and their evaluation

An abdominal aortic aneurysm (AAA) is a bulge in the aorta in the abdomen. AAA is a vascular disease with life-threatening implications, that is becoming increasingly common in aging populations. When the risk of rupture is high, a surgical intervention is required to repair the aorta. The standard approach is the arterial grafting in open surgery, but the mortality of this kind of intervention is high. An alternative to open surgery, recently developed, is the endovascular repair,consisting in the introduction of a prosthesis with a catheter passing through the iliac artery. This procedure can be performed in a surgical or

a radiological suite, but it requires a preliminary accurate assessment of patient's specific anatomy. The measurements of the geometry of the aorta is therefore extremely important. As stated in [Baskin et al., 1996], the true aneurysm diameter and its growth ratio are fundamental parameters to evaluate the risk of a rupture and to compare it with the risk of a surgical intervention. Moreover, if it is decided that surgery is necessary and a prosthesis must be placed, a correct geometrical evaluation of the aneurysm structure is fundamental to have a successful implant. Fig. 3 shows distances and angles that have to be measured with sufficient precision for the planning of the surgical interventions and the selection/design of prostheses.

CT is the most accurate and frequent screening technique [Santilli and Santilli, 1997]. The evaluation of the parameters from the CT slices is, however, usually done with empirical techniques measuring lengths and radii with calipers [Lederle et al., 1995, Baskin et al., 1996]. If the parameters are estimated on the original 2D slices or from other 2D projections, or directly from the trajectory of a catether inserted in the artery, a large amount of error due to the curvilinear structure of the vessel (Fig.2) is introduced both in diameter and length measurements.

Ultrasound imaging is also used for aneurysm quantification; Digital Subtraction Angiography is also used for its high spatial resolution, but provides only two-dimensional information [Blankesteijn, 2000].

Computer assisted volumetric approaches have been proposed and tested, but with complex and proprietary software on visualization workstations (e.g.,[Baskin et al., 1996]). Our models allow a very simple and fast measurement of the required values without the need of particular hardware or software and the measurement of aortic aneurysms seemed a good test-bed to show the usefulness of the approach chosen. Moreover, this technology is ideally suited to support distributed services that improve the measurement quality (using the 3D reconstruction) and allow also collaborative surgical planning between remote sites.

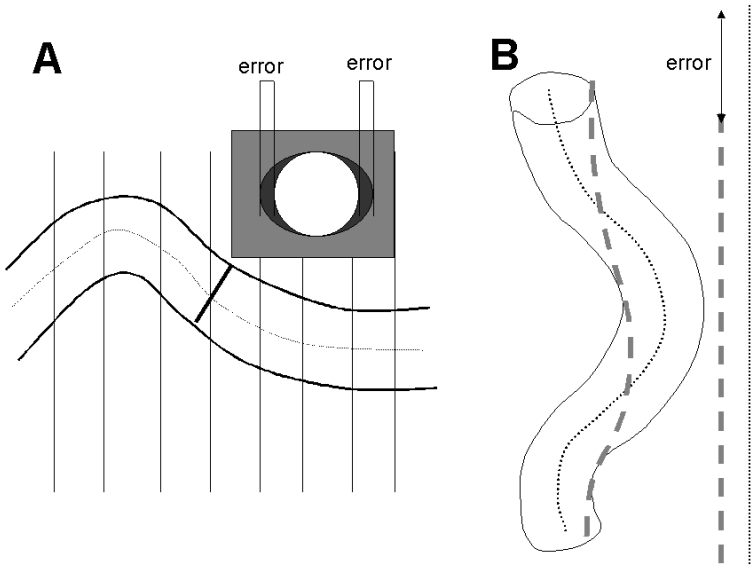

Figure 2: Errors introduced by estimating vessel length and diameter from 2D slices or catheter trajectory. A: the diameter measured from a CT slice can be superestimated is the vessel direction is not perpendicular to the slice plane. B: The vessel length measured from the catheter trajectory is underestimated.

2 Segmentation and 3D reconstruction

2.1 The arterial tree data structure

In order to perform measurements on vascular geometries (and also to support other virtual reality and numerical simulation applications) we designed a specialized data structure that we named "Arterial Tree". An Arterial Tree is defined as the union of a complete surface mesh with no holes describing the vessels internal surface, and a skeleton joining series of 1D lines representing the vessels centerline. This structure allow us to

- realize precise measurements of vessel length;
- simplify the estimate of a plane perpendicular to the vessel;
- provide a geometrical model that can be used to build a volume mesh inside the vessel for numerical simulation of blood flows [Abdulaev et al., 1998]

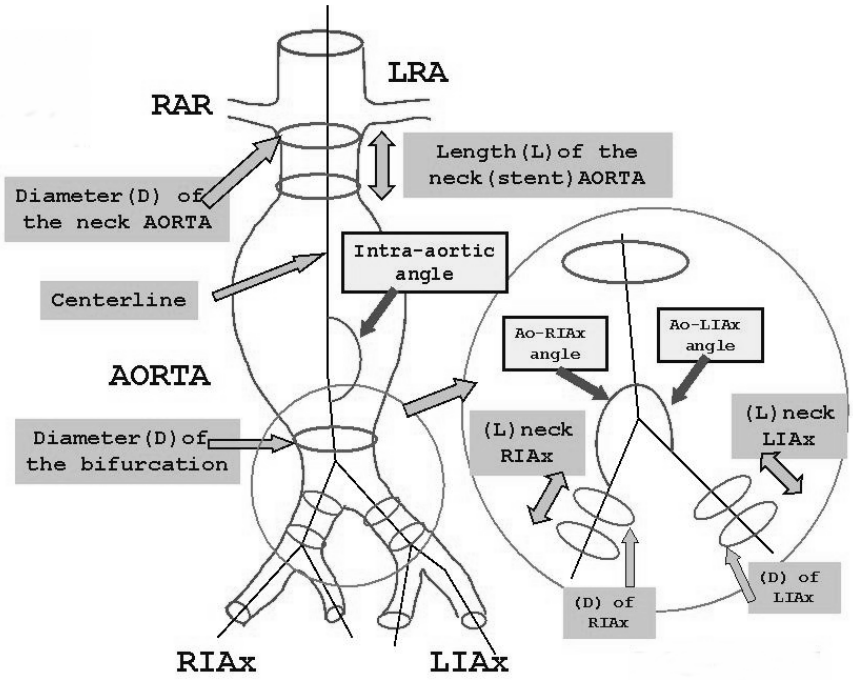

Figure 3: A large number of measurements are necessary, including the length and diameter of the proximal aortic "neck", the length and diameter of the distal "cuffs", and the length of the two graft limbs. Measurements for an endovascular tube graft are only slightly less complex.

We implemented three methods for the reconstruction of the AT structure and developed an user friendly interface to control the use of these methods and other image processing tools (see Fig.4).

Methods are:

- **A:** Segmentation from 2D contours: The dataset is cut with series of planes approximately directed along the vessel branches directions. Contours are extracted with snake balloons and joined in simple tubes. Finally, tubes are glued to build the complete tree. The centerline is built generating a spline passing through the centers of mass of the extracted contours.

- **B:** Segmentation from isosurfaces and automatic centerline extraction: Thresholding and marching cubes are used to compute the vessel surface, while an automatic centerline extraction algorithm initialized by simply giving a point inside the vessel has been implemented.

- **C:** Segmentation from Simplex Balloon and automatic centerline extraction: Simplex balloons are a deformable surfaces in the 3D space. Initializing surfaces as small spheres inside the vessels and choosing the correct forces inflating and driving surface points to the vessel border, we can obtain a smooth vessel surface. The same algorithm as in method B is used for the centerline extraction.

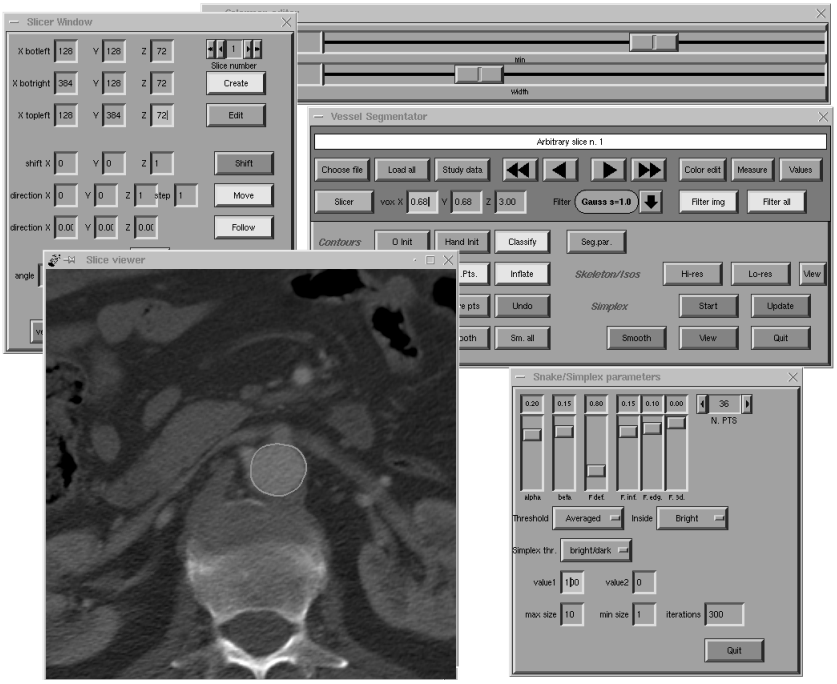

Figure 4: The user interface allowing the easy use and tuning of all the segmentation algorithms implemented.

In the following subsection a detailed description of the methods is given, and in the experimental sections we compare the results obtained with the three methods.

2.2 Method A: Segmentation from 2D slices

The basic segmentation procedure used is summarized in Fig. 5. Series of contours with a fixed number of points are extracted on slices with arbitrary position and orientation in the 3D dataset. Images are computed from the 3D dataset using tri-linear interpolation. The user interface include a menu to select the slices from the dataset and give the possibility of extracting contours with the following methods:

- **Snakes**: Snakes are elastic contours that undergoes a "physical" evolution driven by "forces" [Kass et al., 1988]. A contour is defined as a set of connected labelled points, $\vec{p}(i)$ subjected by external force fields and interact with their neighbors. If forces are chosen correctly, the contour evolution is stopped near the desired image feature. The initial contour can be chosen as a small circle around a selected point, as the contour detected on the previous slice (useful choice to segment vessels), or drawing the approximate position by hand. Usually the first option is used for the starting slice of a series, the second for the other slices, and the third in case of noise or problems in automatic detection. The evolution of our snakes is driven by standard elastic and rigid forces related through the parameters α and β (see [Kass et al., 1988]) to the derivatives of the contour, by an inflating force $\vec{F}_i$, like in [Cohen and Cohen, 1990], by an edge attraction directed as the derivative of the squared local gray level gradient and by a deflating term that makes the contour shrink along the normal vector direction $\vec{n}(i)$ if the image brightness or the difference between the image brightness and the image brightenss corresponding to the contrast medium is above a local threshold T. The threshold can be selected considering the Hounsfield values corresponding to the contrast medium. However, for some of the data analyzed, the contrast was not always perfect and in this case it can be a better choice to use an adaptive algorithm searching for strong discontinuities along the

directions perpendicular to the contour and selecting the corresponding "external" value as threshold.

- **Region growing**:

  If the contrast is good, it is possible to detect the vessel section with a simple region growing algorithm: the user clicks inside the vessel region and sets a gray level threshold and the program detects the connected region including the center with a gray level that differs from the central value less than the threshold value. Finally the algorithm extract the external contour of the detected region and re-sample it with the required number of points. The region growing algorithm has the advantage of requiring less parameter tuning, but snakes are more robust when the contrast is not so good and do not require re-sampling and smoothing after contour extraction.

The major advantage of the contour based approach is that it is immediately visually clear if the algorithm worked well. The user interface provides several post processing facilities to modify the result if necessary:

- Some points can be moved to a different location.

- Contours can be smoothed with a center based algorithm as follows: first one computes the local average distance of the point and two neighbors from the contour center of mass and then the point is shifted in order to have the distance from the center equal to that value. This can be really effective if the contour is not too irregular.

- The number of points can be changed and contours can be re-sampled making the distance between successive points approximately constant. This is done by calculating: the length of a spline joining the points; the corresponding average point spacing; and finally replacing the points along the line.

- Selected points can be marked as "Fixed", and these points are not moved during further application of the snake algorithm.

This manual editing is sometimes necessary if the signal to noise ratio in the images is low, and features such as calcifications are clearly visible but hard to discriminate with the automatic methods.

The selection of the slices is, in the current implementation, manual, even if done through a user friendly inteface where the new slice can be easiliy and fastly created by shifting and rotating the previous one. When the segmentation of a contour series is finished, the user saves all the contours points in a file, then reset the slicer tool and can extract a new series of contour, corresponding to another vessel branch, until all the geometries of his interest are reconstructed.

The second step in the geometry building is the generation of vessel segments. Being each series composed of the same number of contours, evenly spaced, the program automatically finds the correspondence between points of successive contours (as the one minimizing the average distance of points with the same label). Finally, the surface is built joining with edges the neighboring points of each contour and each contour point with the points of the next contour of the series having the same label. The surface is finally triangulated. If smaller triangles are required, it is possible to add other nodes. Finally the vessel centerline is built as a spline connecting the center of mass of the contours.

Once vessel segments are, they are glued together with an anastomosis operation, i.e. the insertion of the secondary branch into the largest one. This is done as follows: first the intersection between the two external surfaces is found, then the part of surface inside the largest vessel is removed and a new triangulation is created near the intersection curve.

Errors introduced in the geometry depend on the number of slices used for the segmentation, if the slices are sufficiently close each other, the error can be considered equal to the voxel dimension. The computed centerline can be exploited for an iterative refinement

of the geometry: first new cutting planes orthogonal to the centerline are generated, then new contours are extracted (Fig 6). Geometrical operations are realized with the support of the XOX Shapes MicroTopology libraries [Xox]. The choice of the geometrical engine, however, is not critical, because the routine used moves or creates nodes only along the intersection of the two surfaces joined and the precision of the library in determining the intersection is three orders of magnitude higher than the contour segmentation.

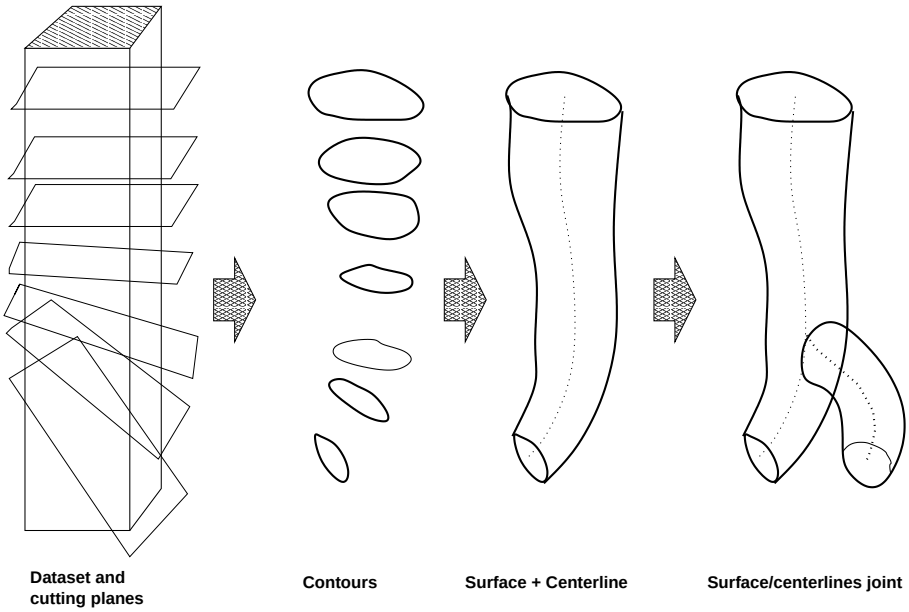

Figure 5: Arterial Tree building from contours and centerlines. Several contour series can be extracted and several vessel segments, with an external surface and a center line are consequently built. Finally they are joined in an unique tree, with only one triangulated surface and a tree-shaped centerline.

2.3 Automatic centerline extraction

Methods B and C are based on surface extraction with Marching Cubes or deformable surfaces. In both cases, to build the AT structure, we have also to find the centerline of the vessel. We therefore have implemented an algorithm for the centerline extraction directly working on the voxel data, where the user has just to select on the first slice a pixel inside the vessel lumen and a threshold value. Then the algorithm, derived from the

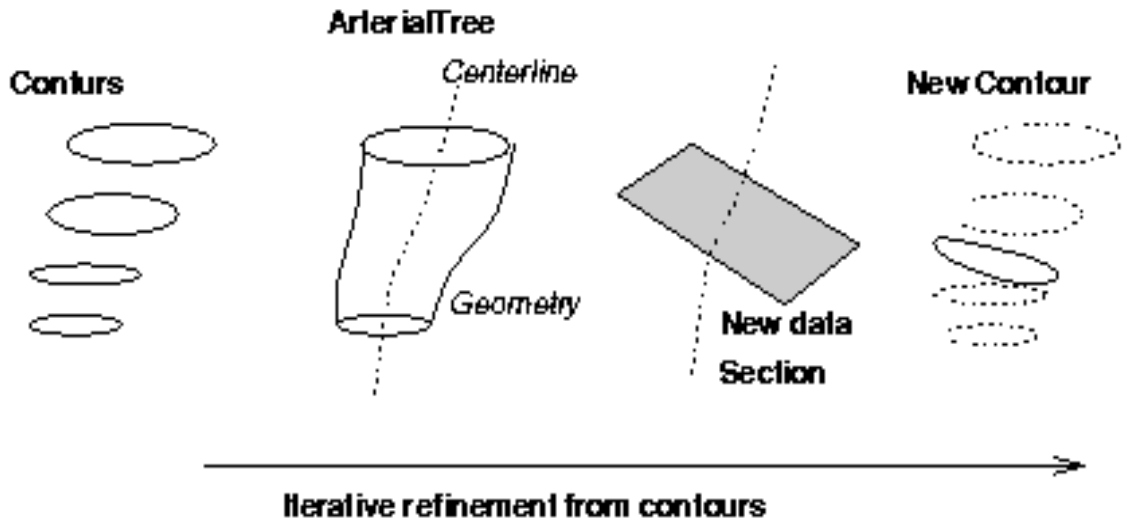

Figure 6: Arterial segments can be refined adding new planes orthogonal to the computed centerline.

voxel coding technique by Zhou [Zhou and Toga, 1999], works as follows:

- Compute a "distance" of each internal point from the connected region boundaries (Boundary seeded distance, BSD).
- Compute a "distance" of each internal point from the starting point of the segmentation or "seed point" (SSD).
- Find maximum of the SSD.
- Starting from the point corresponding to this maximum, create a chain connecting at each step the last detected point with the neighboring voxel with the lowest value of SSD. The chain must end at the seed point.
- For each point of the chain find the connected region with the same SSD. Find the maximum of the BSD in the region and move the chain point there. Put to zero the SSD value of the region. The resulting chain is a vessel centerline branch.

- Find the maximum of the changed SSD map and repeat the same procedure, stopping the chain detection when a voxel with zero SSD is found. The result is a new vessel branch. Repeat the procedure until the SSD is not cleared.

- Branches are finally smoothed and connected.

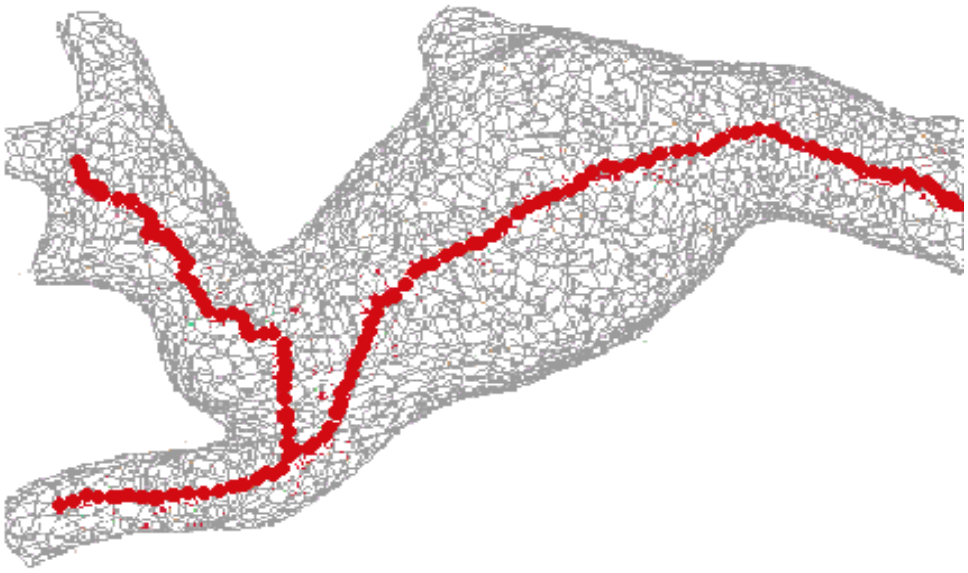

Figure 7: Balloon segmentation of an iliac bifurcation with the corresponding skeleton extracted inside.

2.4 Method B: isosurface extraction

The second option available to the user is the extraction of an isosurface. After a Gaussian or median smoothing, the dataset is binarized and a region growing algorithm is started from the seed given by the user. Finally the marching cubes algorithm [Lorensen and Cline, 1987] is applied.

2.5 Method C: 3D balloon reconstruction

Deformable surfaces can now be used for 3D segmentation due to the improved computational power of PC's and workstations. A survey on their use can be found in [Mc Inrey and Terzopulos, 1996]. Specific applications of have already be presented by other authors, i.e. [Magee et al., 2001], who used also some model based constraint to segment the correct structures. The method here used is based on the simplex mesh geometry introduced by Delingette [Delingette, 1994]. As defined in the paper, the generic Simplex Mesh is a N dimensional mesh with N+1 connectivity. The simplex mesh we use is therefore a closed surface mesh composed by nodes each connected with three neighbors. We make the nodes move under the influence of an inflating force $\vec{F_i}$ directed along the surface normal, an elastic smoothing force described in [Delingette, 1994] ("surface orientation continuity constraint") and two image forces:

-a deflating force directed against the surface normal and compensating the inflating one; its modulus is relevant where the local average of the gray level differs from the internal value more than a fixed threshold;

-an edge attraction moving nodes towards the maximum of the gray level gradient modulus in the neighboring.

Controls on maximum and minimum of the face size have been introduced to have the desired mesh refinement. We used also the methods to collapse or divide faces of the mesh well described in [Delingette, 1994]. The final mesh is converted in the "Dual" form (i.e. a new mesh with nodes in the center of the simplex faces and connections corresponding to the simplex edges, see Fig8), in order to have a smooth triangulation to be rendered. The simplex mesh, in fact, due to its definition, is in general composed by polygons that are not necessarily planar, and therefore cannot be easily represented.

In order to use this method, the user must click on a point inside the vessel lumen. The surface is then initialized as a small sphere and is inflated until the surface is not blocked

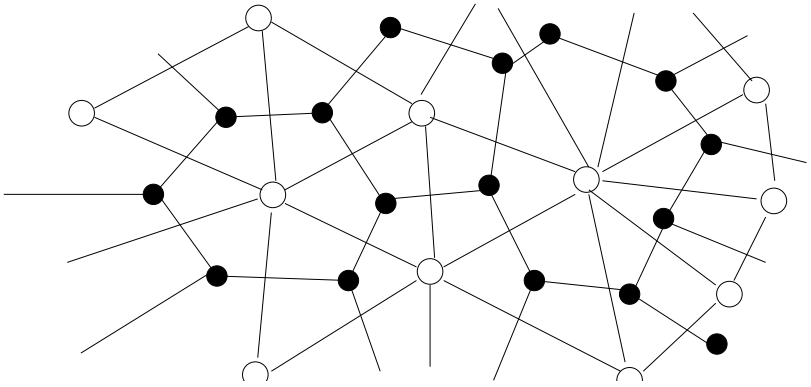

Figure 8: A simplex mesh (black nodes) and its dual triangulation (white nodes)

by edges or changed image value. The user can control the maximum number of iterations to be performed, force parameters and the maximum and minimum size of the polygons. A possible alternative is to use the dual of an isosurface to initialize the simplex near the correct boundaries and to extract a smoother surface.

2.6 Smoothing an ArterialTree

If the 3D surface is reconstructed with an isosurface extraction or with 2D contours the resulting surface may require a regularization. To smooth the ArterialTree we use the "distance from centerline" algorithm: we move each point to the average position of the neighboring and then we move it along the direction of the normal vector in order to have the distance from the centerline equal to the local average distance from the centerline. If $\vec{d_i}$ is the distance from the nearest centerline point $\vec{C_i}$ of the node $\vec{P_i}$, the smoothed node is given by:

$$\vec{P'}_i = \vec{C}_i + \frac{\sum_{j \in neigh(i)} \vec{d_j}}{n\_neigh(i)} \tag{1}$$

This makes the surface regular without shrinking it. Fig. 9 shows an example of the effectiveness of the method proposed.

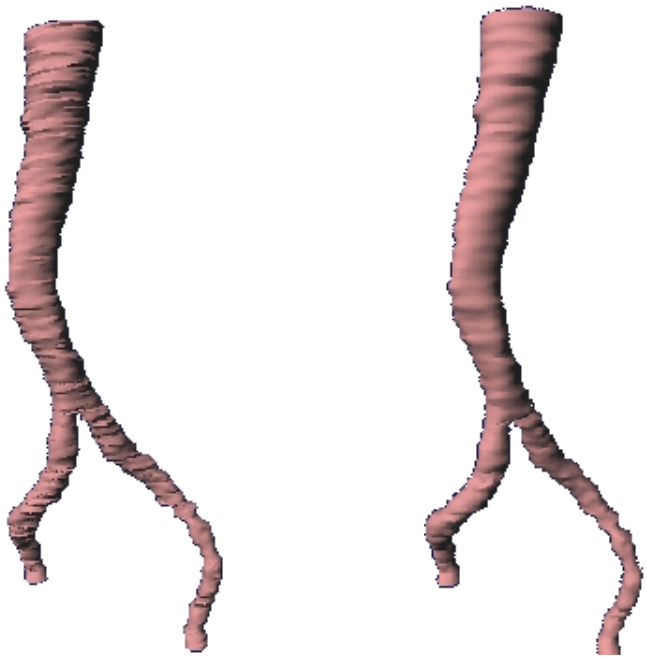

Figure 9: Effects of centerline smoothing on a iliac bifurcation reconstruction.

3 VRML97 measurable models of AAA

VRML97 is a powerful language to describe 3D scenes and it is the standard language for Virtual Reality on the web. VRML97 plug-ins for Internet Explorer and Netscape Communicator (i.e. Cosmo Player [Cosmo Software] are available on the net and can be downloaded with no charge. We tested our code with Cosmo Player 2.1 for Microsoft Windows 98/NT both with Netscape and Internet Explorer. Using VRML97 we converted models of arterial trees representing abdominal aortic aneurysm introducing code to perform through the browser all the measurement useful to surgeons.

3.1 VRML97 translation of Arterial Trees

Here are some details about our data conversion: VRML97 worlds are generated automatically from the Arterial Trees structure. Different "nodes" of VRML97 have been used to represent the geometry of the vessel surface (`IndexedFaceSet`) and the vessel centerline

(`IndexedLineSet`); The centerline is also duplicated alone in another part of the scene alone to make easier the measurement of angles and distances. The Viewpoint node is used to define a set of privileged points of view (at the end of each vessel branch and an external global view). The `TouchSensor` node have been used to let the user interact with the geometries; we exploited it not only to get the coordinates of the vessel, but also to create buttons to select the possible actions to be done. The `Timer` node have been also used to create animations because it changes the value of an output variable as defined by the programmer. Routing the output of a `Timer` to other nodes called `PositionInterpolator` and `OrientationInterpolator` that give, as suggested by the name, a series of values of coordinate and direction, we can control the the motion of the point of view in order to create a driven navigation along a fixed path. Our conversion script creates automatically a guided navigation along each branch of the tree along the vessel centerline.

3.2 Support for measurements

The VRML97 language specification includes a particular node, called `Script`, that is extremely powerful. It makes possible when another node creates an event, to call a custom ECMAScript or Java routine written directly on the VRML file or saved to a linked one. The routine can take as input values depending on the scene and on the user actions and output values can be routed to the other nodes.

Using ECMA scripting we implemented three methods to measure parameters useful for medical applications.

The first consists of printing the 3D coordinates and the distance from the centerline for each point of the surface when the mouse is clicked on it. A plane perpendicular to the centerline is also shown for an easy control of the distance direction (Fig. 10).

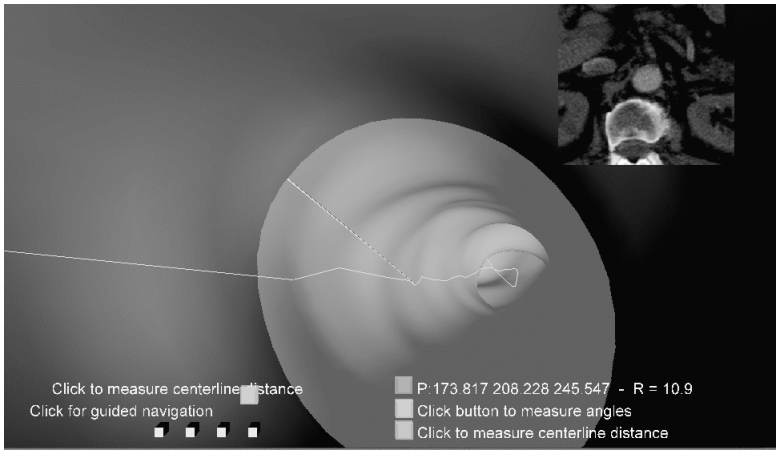

Figure 10: The VRML97 model can be inspected, navigated and measured from any PC with a web browser and a plug-in. Here a "virtual endoscopy" with radius measurement is shown.

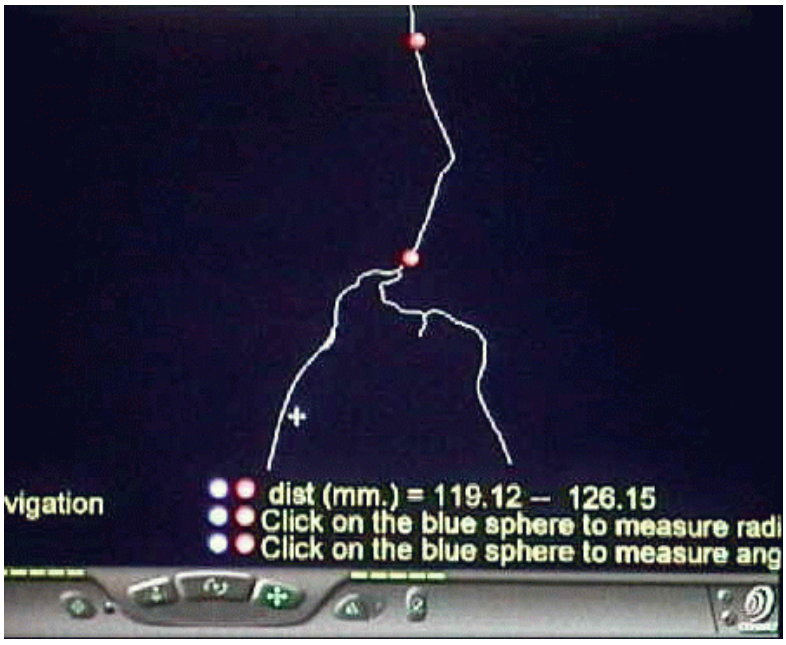

Figure 11: Measurement of centerline distance: the user just clicks on two points on the centerline, and on the browser are automatically displayed the distance between the points and the distance between the points following the centerline, that can be extremely different and it is the really important parameter to evaluate for aneurysm measurements.

Figure 12: Measurement of centerline angles: the user can place the three reference points just by clicking with the mouse on the centerline, and the angle is automatically shown.

The second consists of measuring the distance of two points on the centerline following the line itself (Fig. 11). This is very important, because usual measurements of vessel length done with 2D imaging or endoscopy are often wrong due to the effect of vessel curvature [Baskin et al., 1996, Fillinger, 1999].

The last one is the measurements of angles clicking on three points on the centerline (Fig. 12). Furthermore, we added to the scene an image viewer so that when a point on the surface or on the centerline is clicked for measurement, the image defined by the intersection of the plane perpendicular to the centerline and passing through the point clicked and the dataset is automatically shown. Images are created off-line, compressed ad stored in a common directory on the server side. Being very small they can be downloaded quickly. However, it is possible also to change the code to have them pre-loaded on the client side. Another useful tool introduced in the models is an automatic test aimed at checking if a probe of fixed diameter can pass through the lumen.

4 Experimental results

4.1 Comparison of segmentation techniques

We tested the three segmentation methods described in Section 2 on different CT data sets coming from the Radiology dept. of the University of Pisa and from the Hospital of Ravenna. On datasets obtained following the standard protocols for abdominal aortic aneurysm repair planning, the resolution is less than 2 mm. in the z direction and signal to noise ratio is high: all three methods perform well and the measurements are consistent (see Fig. 13 and Table 1).

Testing the reconstruction on image data acquired not following the standard protocol, we encountered some problems due to poor contrast and lower values of z resolution. A large slice spacing makes difficult to have a smooth surface and even an unique surface for small vessels in the isosurface extraction. A poor signal to noise ratio causes a difficult threshold setting for discriminating the vessel lumen from the background and make often not possible to distinguish automatically calcium from contrast. This means that, even using median filtering and morphological closing, we cannot get automatically a good detection of the lumen and, in some cases, we obtain discontinuous surfaces and false detections of borders. Examples of bad reconstructions are represented in Fig 15. It must be also considered that local errors are likely to be present in reconstructions. For the contour-based reconstructions, errors can be present near bifurcations, even if the image quality is good, due to possible approximation in triangulation methods. 3D balloons are affected by the necessity of finding equilibrium between image based and elastic forces, and can fail in regions where curvature is quite high and signal to noise ratio is low. These errors do not affect, usually, the measurement of the parameters of surgical interest. Some notes must be done also on the time required by the elaborations. Automatic methods require several minutes to extract geometries, but no interaction. The contour based method

requires more time (up to 1-2 hours) with constant user-interaction, but ensuring in this way that the segmentationis more controlled. Errors in the 3D approach must be corrected by repeating all the segmentation procedure.

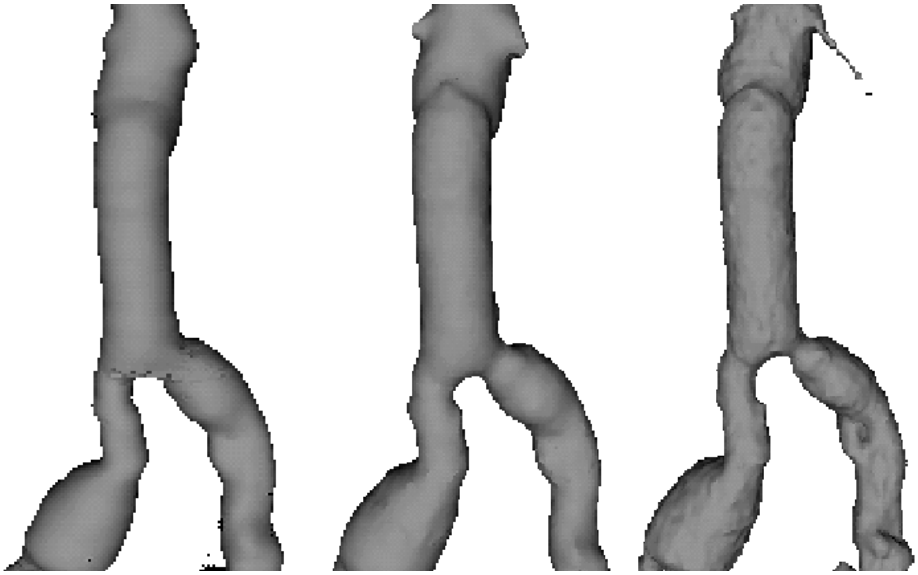

Figure 13: Comparison of the three reconstruction methods on a sufficiently good acquisition. Left: Reconstruction performed through 2D contour extraction. Center: Reconstruction performed using Simplex balloon and automatic centerline extraction. Right: Reconstruction performed using marching cubes and automatic centerline extraction.

Measure	Method A	Method B	Method C
Neck radius (mm.)	11.8 ± 0.7	11.9 ± 0.7	11.4 ± 0.7
Maximum aneurysm radius (mm.)	15.4 ± 0.7	16.0 ± 0.7	16.2 ± 0.7
Length (mm.)	115 ± 2	115 ± 2	115 ± 2

Table 1: If the image quality is good, measures of parameters performed on the three models are compatible. Here are, for example the results of corresponding measurements on the three models of Fig. 13.

4.2 Sensitivity to initialization and parameters change

As in all the segmentation techniques, the results obtained with our method are influenced by thresholds and parameters choices (α, β, $\vec{F_i}$ T, etc..), i.e, they are user dependent. The results obtained with our methods are, for instance, strongly dependent on the gray level

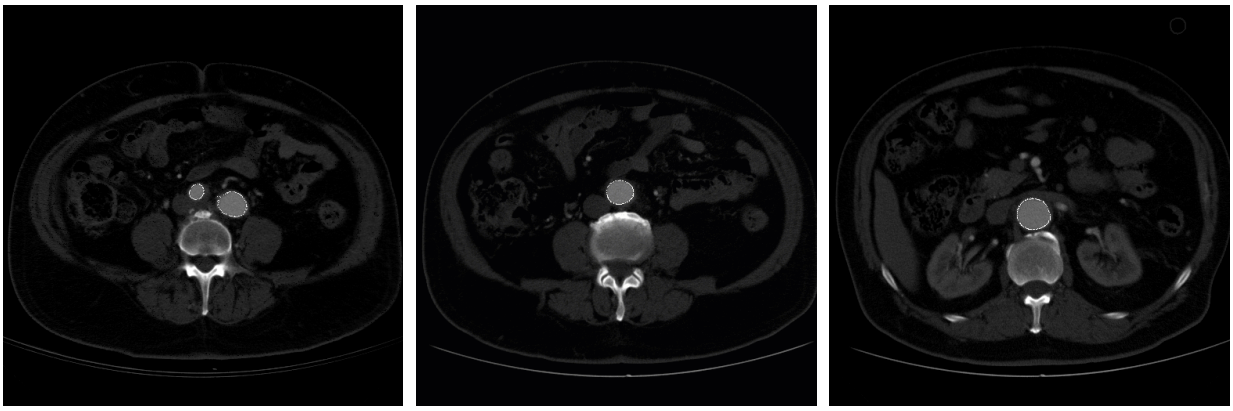

Figure 14: If the image quality is good, simplex points displayed over the corresponding image are placed in the correct position.

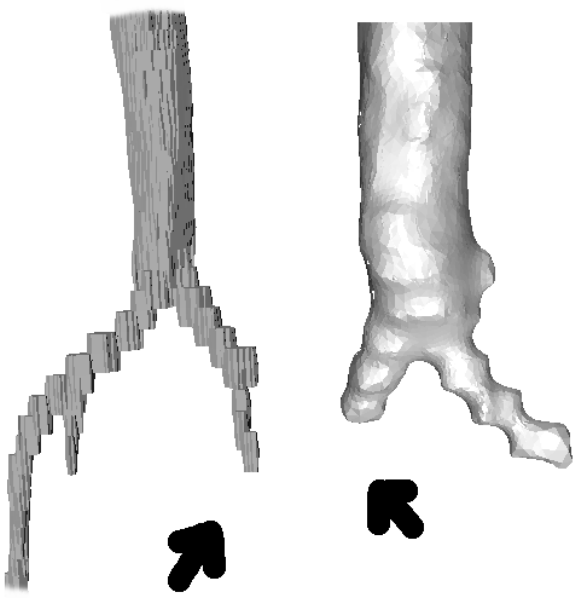

Figure 15: Problems due to the poor resolution: it is difficult or not possible to extract small and tortuous vessels. In this case slices were spaced by 7 mm.

thresholds and on the values of elastic parameters. We found, however, our method only weakly dependent on the initialization point, both for 2D and 3D methods. Different gray or edge threshold or a different elastic constant can change the segmentation result and thus these parameters should be selected under the supervision of an expert radiologist with a non trivial experience in segmentation, because even if many of the program options are automatic or semi-automatic, the user needs to have a feeling of the algorithms and of images features in order to perform a better reconstruction. This fact suggests of the usefulness of our approach that allows the 3D reconstruction to be outsourced to a centralized reconstruction center.

4.2.1 Sensitivity issues for 2D methods

Region growing result depends only on the choice of the threshold, so the selection of a reasonable protocol is sufficient to guarantee user independence. The behavior of a snake can be changed in many ways, acting on elastic parameters, force constants, the number of points chosen, and so on. This means that the segmentation result depends on the user's choices. This is not a drawback: it makes possible, acting on that parameters, to segment different structures on different kind of images. The user dependency can be, however, controlled, by using, for each kind of task required, a detailed protocol giving a parameters set for the contour extraction. For CT images like those in 14, a possible protocol is:

- Perform 3x3 median filtering.
- Select a correct windowing to show the desired structures.
- Choose a sufficient number of points in order to have a point spacing of a few pixels.
- Use an image force selecting a bright region in dark background with a fixed threshold and the elastic and force constants saved after tuning for these kind of segmentation.

Case	avg. cont. diff./voxel size	max cont. diff./voxel size
snake/snake	0.16	0.51
reg. growing/snake	0.20	0.62
manual/snake	0.24	1.58
simplex section/snake	0.33	0.91
isosurface section/snake	0.47	1.38

Table 2: Comparison of segmentation results obtained by different users with different techniques: the table shows the average and maximum distance between points belonging to different snakes segmentation, distances between a contour obtained with region growing and one obtained with snakes, between a contour drawn by hand and a snake segmentation, between snake points and a simplex mesh and between snake points and an extracted isosurface.

- Initialize the contour inside the region letting it evolve until the contour motion is stopped.

- re-sample the contour to have the desired number of points equally spaced.

Once the protocol is defined, our goal is to prove that the result do not depend on the contour initialization, i.e. once the parameters are set, the method is user-independent. We selected five slices with differently shaped vessel sections and measured the averaged distances between points of contours extracted with different methods and with and between five snakes results obtained with a different initial contour positioning. Results(see Table 2) show clearly that when the contour is well defined, the contour extraction is user-independent, and the differences between the segmentation techniques are not relevant.

Only if the image quality is bad, for example when the contrast is low (Fig. 16) there is no way to use the standard parameters obtaining a user-independent result. The user, in this case, must draw the contour by hand or correct the result where not reliable (for example near plaques or artifacts). This fact underlines the importance of having an experienced person doing the segmentation work, and this should be considered a specialized task even if performed with user friendly software.

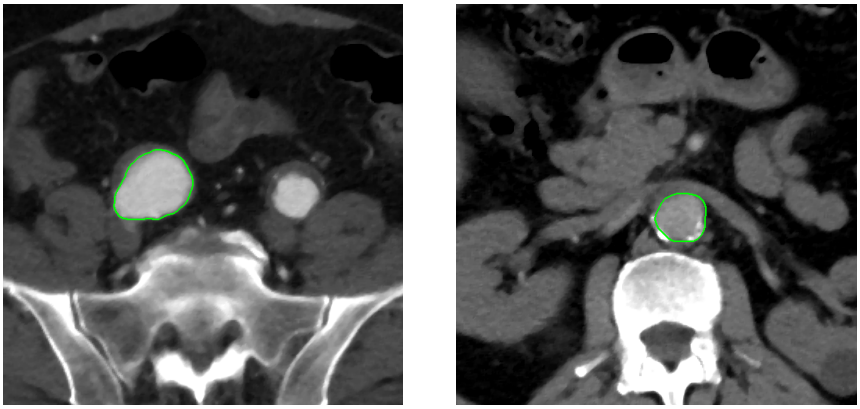

Figure 16: Left: One of the slices use to test the user independence of the system when the image acquisition is correct. Right: One of the slices where the contrast is too poor to have user independent results due to bad image acquisition

4.2.2 Sensitivity issues for 3D methods

If a fixed threshold is chosen, a comparison between balloon isosurface and manually selected contours or 2D snakes is possible. Fig. 17, for example, shows the nodes of a simplex balloon lying on a CT slice, superimposed to the corresponding gray values and the corresponding 2D snake.

We performed this comparison on all the data sets and we have found that for images acquired using standard protocols the two reconstructions are consistent at the voxel level, i.e. the distance between corresponding points in different reconstructions is always lower than the voxel size.

4.3 Parameter estimation form VRML models

We have finally taken 12 models of aortic aneurysm from CT data provided us by the Radiology dept. of the University of Pisa and from the Hospital of Ravenna, and chosen selected parameters to be measured with a standard 2D technique and with the VRML browser. The parameters are:

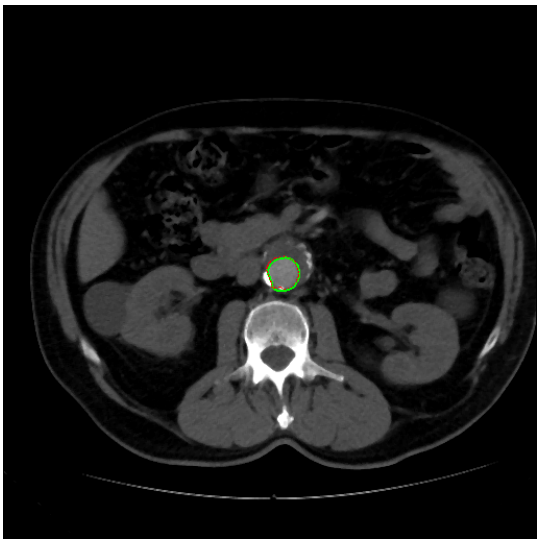

Figure 17: If image quality is good and vessel structure is simple, points from contour segmentation and from a 3D model (in this case Simplex based) sections are correctly superimposed: no relevant differences are visible between the two contours printed over the image

- Radius of the aortic neck
- Length of the aneurysm
- Intra-aortic angle
- Radius of the bifurcation

Being some of the cases analyzed in the test poor in contrast or resolution, we decided to adopt as standard segmentation method for the VRML97 generation the 2D contour based segmentation. The comparison has been realized in the following way: for the vessel radius, the doctor working on the CT slices measured transversal and axial radii, the other working on the VRML measured in four selected vessel points at the same z location, the distance between the point and the centerline, taking the average value as the correct radius. We gave as error to all the measures the voxel size in x,y directions.

Case	Axial r.(mm.)	Transversal r.(mm.)	VRML min r.(mm.)	VRML max r.(mm.)
1	10.6 ± 0.7	11.6 ± 0.7	11.2 ± 0.7	12.1 ± 0.7
2	10.4 ± 0.7	10.1 ± 0.7	8.9 ± 0.7	10.9 ± 0.7
3	16.8 ± 0.7	18.5 ± 0.7	17.8 ± 0.7	19.0 ± 0.7
4	9.9 ± 0.7	10.3 ± 0.7	9.9 ± 0.7	10.5 ± 0.7
5	12.5 ± 0.7	15.6 ± 0.7	11.8 ± 0.7	12.8 ± 0.7
6	11.0 ± 0.7	11.6 ± 0.7	11.0 ± 0.7	11.5 ± 0.7
7	10.3 ± 0.7	11.3 ± 0.7	9.2 ± 0.7	10.7 ± 0.7
8	13.4 ± 0.7	12.3 ± 0.7	12.5 ± 0.7	12.7 ± 0.7
9	10.3 ± 0.7	10.6 ± 0.7	9.7 ± 0.7	10.3 ± 0.7
10	13.0 ± 0.7	10.6 ± 0.7	9.3 ± 0.7	12.4 ± 0.7
11	9.7 ± 0.7	9.7 ± 0.7	8.9 ± 0.7	9.7 ± 0.7
12	11.6 ± 0.7	10.3 ± 0.7	10.3 ± 0.7	10.9 ± 0.7

Table 3: Radius of the aortic neck (measured carefully at the same z location using a standard 2d method, and working directly on the 3D model

Case	Axial r.(mm.)	Transversal r.(mm.)	VRML min (mm.)	VRML max (mm.)
1	9.9 ± 0.7	11.6 ± 0.7	10.4 ± 0.7	12.0 ± 0.7
2	9.0 ± 0.7	6.5 ± 0.7	6.3 ± 0.7	8.1 ± 0.7
3	12.1 ± 0.7	18.1 ± 0.7	11.3 ± 0.7	14.1 ± 0.7
4	15.7 ± 0.7	20.2 ± 0.7	15.0 ± 0.7	18.2 ± 0.7
5	12.1 ± 0.7	12.8 ± 0.7	11.8 ± 0.7	12.9± 0.7
6	14.0 ± 0.7	19.8 ± 0.7	13.5 ± 0.7	21.8 ± 0.7
7	22.6 ± 0.7	38.1 ± 0.7	21.4 ± 0.7	26.6 ± 0.7
8	14.0 ± 0.7	15.1 ± 0.7	14.2 ± 0.7	17.2 ± 0.7
9	10.3 ± 0.7	12.7 ± 0.7	8.6 ± 0.7	11.5 ± 0.7
10	6.9 ± 0.7	9.3 ± 0.7	7.3 ± 0.7	7.4 ± 0.7
11	4.5 ± 0.7	17.1 ± 0.7	7.6 ± 0.7	13.5 ± 0.7
12	13.4 ± 0.7	16.4 ± 0.7	12.6 ± 0.7	16.3 ± 0.7

Table 4: Aortic radius near the iliac bifurcation (measured at the same z location) using a standard 2d method, and working directly on the 3D model.

Case	Z distance(mm.)	Length (VRML) (mm.)
1	106 ± 2	115 ± 2
2	88 ± 2	94 ± 2
3	88 ± 8	101 ± 8
4	110 ± 2	120 ± 2
5	120 ± 2	137 ± 2
6	129 ± 5	166 ± 5
7	164 ± 3	170 ± 3
8	129 ± 3	146 ± 3
9	125 ± 5	148 ± 5
10	120 ± 3	133 ± 3
11	110 ± 3	133 ± 3
12	120 ± 3	127 ± 3

Table 5: Z component of aneurysm length and real length measured on the VRML models. It is possible to understand the importance of using a 3D approach, allowing the correct measurement of the vessel length.

Case	Angle (grad)	VRML estimation (grad)
1	139 ± 12	155 ± 12
2	127 ± 12	163 ± 12
3	128 ± 12	135 ± 12
4	145 ± 12	141 ± 12
5	135 ± 12	139 ± 12
6	117 ± 12	125 ± 12
7	124 ± 12	130 ± 12
8	140 ± 12	157 ± 12
9	131 ± 12	130 ± 12
10	136 ± 12	148 ± 12
11	139 ± 12	143 ± 12
12	132 ± 12	139 ± 12

Table 6: Estimation of intra-aortic angle performed by a trained surgeon from 2D slices (left) and using the VRML browser (right).

The results are good. Measurements of radii and angles give more or less the same results, and the correlation between the average radii ath each vertical location with the two methods are strongly correlated (r=0.96). Only in a few cases there are inconsistencies: i.e there are measurements where the difference between the radius estimated with the 2D approach and the radius measured with our method differs for mre than twice the measurement error (cases 3,4,7,11). These discrepancies are, in our opinion, due to an incorrect 2D estimate due to the vessel tortuosity. Errors appear to depend not only on the vertical resolution but also on vessel tortuosity. By looking at the reformatted image displayed on the browser it is possible to check the local quality of the reconstruction (see Fig.18).

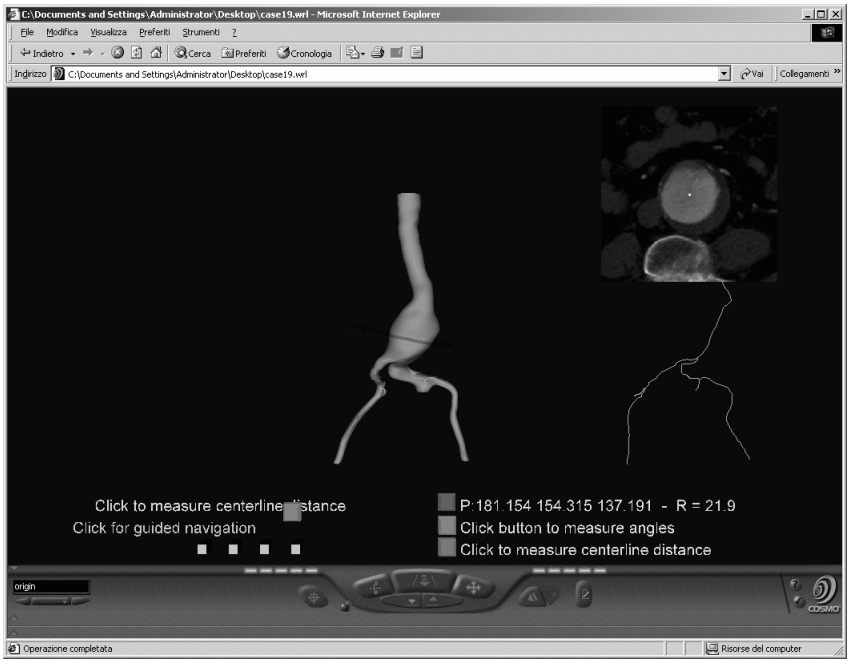

Figure 18: The pre-computed image displayed on the top left represents the reformatted slice (i.e. perpendicular to the vessel centerline), passing near the clicked point.

5 Discussion

Computer vision, virtual reality and Web technologies can really have clinically relevant applications. In this paper we presented a novel application using customized image processing technique and web technologies to help surgeons in diagnosis and pre-operative measurements of 3D structures. The application is simply to be considered as an example showing that the accuracy requested by the application is achievable with these methods, but other applications can be obtained easily.

While the creation of interactive models is something new, the image processing methods are custom versions of well known techniques. We compared the results obtained with different methods, like contour based segmentation, isosurface extraction and 3D simplex balloon inflation. The results suggest that for images acquired using standard protocol, results are equivalent. However, if the quality of images is not perfect it is better to use the more interactive and robust method, like the contour-based, with a strong control by experienced radiologists. Our contour-based approach presents, however, some advantages if compared with other found in literature, for example in [Milner et al., 1998] where segmentation of contours was used to build tubes, but only on the original MR slices and not on arbitrary slices of the 3D dataset.

The remote analysis of the 3D models seems extremely promising: in fact, the system allows inspections and measurement necessary for the planning of surgical interventions and it is:

- Fast: The VRML measurable models can be published on the net within a few hours from the acquisition, independently from the location of the diagnostic and reconstructing centers. Model download is not usually a problem, being our VRML files sufficiently small: a geometry with 10.000 nodes is stored in a file of about 1MB,

that can be gzip compressed to about 300 K, the size of a common image.

- Reliable: almost all the image processing techniques used have been tested in different contexts and applications; the preliminary tests shows also a good accuracy of the measurements if compared with other methods.

- Easy to use: measuring diameters and distances is just done by clicking with the mouse on a browser window and do not require off line calculations or post processing.

We think also that an approach where the segmentation is performed carefully in a controlled environment can give better results than the use of a simple algorithm as those introduced in the CT consoles by personnel not trained for the specific task.

We plan now to test extensively the reconstruction method and to apply a similar approach to different surgical applications. Colonoscopy is, for example, another field of application where this kind of models can be extremely useful for collaborative study or diagnosis.

In order to have a better validation it will be also necessary to test the measurements results on known phantoms, and w plan to do this in the future. A gallery of demo 3D measurable models is available on our web site (http://www.crs4.it/$\simeq$ giach). The work presented here is the basis for the trial EU funded project AQUATICS (IST-1999-20226 EUTIST-M/WP12). For details, see the project web site: http://aquatics.crs4.it.

Acknowledgements

Special thanks to E. Piccinini, M.D., Ospedale di Ravenna, E. Neri, M.D., Università di Pisa for providing data and medical suggestions, and M. Camba for technical help.

References

[Abdulaev et al., 1998] G.Abdulaev, S.Cadeddu, G.DeLussu, M.Donizelli, L.Formaggia, A. Giachetti, E.Gobbetti, A. Leone, C. Manzi, P.Pili, A.Scheinine, M. Tuveri, A.Varone, A.Veneziani,G.Zanetti and A.Zorcolo, " ViVa: The Virtual Vascular Project" IEEE trans. on Information Technology in medicine, 14: 1 34–48 (1998)

[Baskin et al., 1996] K. M. Baskin et al., "Volumetric Analysis of Abdominal Aortic Aneurysm", Medical Imaging 1996: Physiology and Function from Multidimensional Images, Eric A. Hoffman, Editor, Proc. SPIE 2709, p. 323-337 (1996).

[Blankesteijn, 2000] Blankesteijn, J.D., Imaging techniques for endovascular repair of abdominal aortic aneurysm. Medica Mundi 44/2 November 2000

[Brelstaff et al., 2000] G. Brelstaff, S.Moehrs, P.Anedda,M.Tuveri,G.Zanetti, "Electronic patient records on the Java infobus" In Proceedings of PAJAVA 2000 Conference, Manchester, UK. April 2000

[Cohen and Cohen, 1990] L.D. Cohen and I. Cohen, "A finite element method applied to new active contour models and 3D reconstructions from cross-sections" Proc. of 3rd Int. Conf. on Comp. Vision, pp. 587–591 (1990).

[Cosmo Software] Cosmo software, http://www.cai.com/cosmo/

[Delingette, 1994] H. Delingette, "Simplex meshes: a general representation for 3d shape reconstruction", *in CVPR94*, pp. 856–859, 1994.

[Fillinger, 1999] M. Fillinger, "New Imaging Technologies in Endovascular Surgery" Surgical Clinics of North America **79**: 3 (1999)

[Gering et al., 2001] D. Gering, A. Nabavi, R. Kikinis, N. Hata, L. Odonnell, W. Eric L. Grimson, F. Jolesz, P. Black, W. Wells III. "An Integrated Visualization System for

Surgical Planning and Guidance Using Image Fusion and an Open MR" Journal of Magnetic Resonance Imaging, Vol 13, pp. 967-975, June, 2001.

[John et al., 1999] N.W. John, N. Philips, R. Vawda, J. Perrin, "A VRML simulator for Ventricular Catheterisation" in Proceedings of the Eurographics UK conference, Cambridge, UK, April 1999

[Kass et al., 1988] A. Kass, A. Witkin and D. Terzopoulos, "Snakes: Active contour models," Int. J. of Comp. Vision **1,** 321–331 (1988).

[Krissian et al., 1998] K. Krissian et al. "Model Based Multiscale Detection and Reconstruction of 3D vessels" INRIA Sophie Antipolis Report n.3442 (1998)

[Laxminarayan, 2000] S. Laxminarayan editor, "Information Technology Applications in Biomedicine, 2000. Proceedings".

[Lederle et al., 1995] Lederle FA, Wilson SE, Johnson GR, Reinke DB, Littooy FN, Acher CW, Messina LM, Ballard DJ, Ansel HJ. Variability in measurement of abdominal aortic aneurysms. Journal of Vascular Surgery 1995; 21:945-52.

[Lorensen and Cline, 1987] W.E. Lorensen and H. E. Cline, "Marching cubes: a high resolution 3D surface construction algorithm". In M.C. Stone ed., SIGGRAPH '87 Conference Proceedings, pp. 163–170 (1987).

[Magee et al., 2001] D. Magee, A. Bulpitt, E. Berry, "3D Automated Segmentation and Structural Analysis of Vascular Trees Using Deformable Models" Proc. IEEE Workshop on Variational and Level Set Methods in Computer Vision, 2001.

[Mc Inrey and Terzopulos, 1996] T. Mc Inrey and D. Terzopulos, "Deformable models in medical image analysis, a survey" Medical Image Analysis, 1(2): 840–850, 1996

[Medical Media System, 2000] Medical Media Systems, http://www.medicalmedia.com

[Milner et al., 1998] J.S. Milner et al. "Hemodynamics of human carotid artery bifurcations: computational studies with models reconstructed from magnetic resonance of normal subjects ." J. of Vascular Surgery, 07/1998, pp.143–156

[Parodi et al., 1991] J.C. Parodi, J.C. Palmaz, H.D. Barone, "Transfemoral intraluminal graft implantation for abdominal aortic aneurysms" Ann Vasc Surg 1991;5:491-499.

[Piqueras and Carreño, 1998] J. Piqueras, J.C. and Carreño editors "EuroPacs 1998 Conference proceedings" Barcelona, 1998

[Santilli and Santilli, 1997] J.D. Santilli and S. M. Santilli, "Diagnosis and treatment of Abdominal Aortic Aneurysms" American Family Physician 56:4 (1997)

[Sato et al., 1997] Sato, Y et al, "Evaluation of intracranial aneurysms with CT angiography: current status and future direction", In SPIE Proceedings Vol. 3033 Medical Imaging 1997: Physiology and Function from Multidimensional Images

[Tillich et al., 2001] Tillich M, Hill BB, Paik DS, Petz K, Napel S, Zarins CK, Rubin GD., "Prediction of aortoiliac stent-graft length: comparison of measurement methods." Radiology 2001 Aug;220(2):475-83

[Vital Images] Vital Images www.vitalimages.com

[Voxar] Voxar Plug'n view www.voxar.com

[Xox] XOX Corporation, http://www.xox.com

[Zhou and Toga, 1999] Y. Zhou and A. W. Toga, "Efficient skeletonization of volumetric objects", *TVCG*, vol. 5, 1999.